Bioactive Materials 4 (2019) 37–42

Contents lists available at ScienceDirect

Bioactive Materials

journal homepage: http://www.keaipublishing.com/biomat

Powder metallurgical Ti-Mg metal-metal composites facilitate osteoconduction and osseointegration for orthopedic application

Sihui Ouyang[a], Qianli Huang[a,*], Yong Liu[a,**], Zhengxiao Ouyang[b], Luxin Liang[a]

[a] State Key Lab of Powder Metallurgy, Central South University, Changsha, 410083, PR China
[b] Department of Orthopedics, The Second Xiangya Hospital, Central South University, Changsha, Hunan, PR China

ARTICLE INFO

Keywords:
Powder metallurgy
Composites
Osteoconduction
Osseointegration

ABSTRACT

In this work, Ti—Mg metal-metal composites (MMCs) were successfully fabricated by spark plasma sintering (SPS). In vitro, the proliferation and differentiation of SaOS-2 cells in response to Ti—Mg metal-metal composites (MMCs) were investigated. In vivo, a rat model with femur condyle defect was employed, and Ti—Mg MMCs implants were embedded into the femur condyles. Results showed that Ti—Mg MMCs exhibited enhanced cytocompatibility to SaOS-2 cells than pure Ti. The micro-computed tomography (Micro-CT) results showed that the volume of bone trabecula was significantly more abundant around Ti—Mg implants than around Ti implants, indicating that more active new-bone formed around Ti—Mg MMCs implants. Hematoxylin-eosin (H&E) staining analysis revealed significantly greater osteointegration around Ti—Mg implants than that around Ti implants.

1. Introduction

Titanium (Ti) and its alloys have been widely employed for bone replacement due to their good mechanical properties and corrosion resistance [1–3]. However, Ti is known to be non-osteoinductive. Unsatisfying and unsufficient osteointegration of the implanted Ti with surrounding bone tissue still remains as a great challenge at the early stage of implantation [4–6]. Therefore, improving the in vivo performance of Ti implants after implantation is required. Particularly, the bone healing efficiency related to Ti implants needs to be improved. Moreover, desired biological performances of implants are mandatory, involving bioactivity, osteoconduction and osseointegration.

Mg and its alloys with excellent bioactivity are potential candidates for biodegradable metallic implants [7–9]. In particular, Mg—Zn alloys exhibited good histocompatibility, the released Mg^{2+} and Zn^{2+} are both essential elements in human body which can promote bone formation and mineralization [10–12].

To improve the bioactivity of Ti, the further modification of Ti is one of the most active research areas [13]. Several techniques have been developed to fabricate Ti—Mg composites through the combination of Ti and Mg, such as infiltration, extrusion and spark plasma sintering (SPS) [14–16]. The SPS technique utilizes a pulsed direct current simultaneously with an uni-axial pressure to sinter powders [17]. This process is normally characterized by rapid heating rate and short sintering time [18]. Due to these favorable characteristics, SPS is considered as a promising method for the manufacturing of MMCs. Previous results indicate that Ti—Mg composites improved the bioactivity of Ti, and the Ti—Mg composites possessed good biocompatibility to osteoblasts [16]. However, the in vivo osteoconductivity and osseointegration of the Ti—Mg MMCs still remain to be investigated. It is of great importance to explore that whether Ti—Mg implants show greater capability in up-regulating the osteogenic activity of SaOS-2 cells than Ti implants, and if the bone tissue could grow into the pores of implanted Ti—Mg.

In this work, Ti—Mg MMCs were fabricated by SPS. In vitro and in vivo experiments were conducted on Ti—Mg MMCs to investigate the biological performances. Particularly, the in vitro alkaline phosphatase (ALP) activity of SaOS-2 cells was evaluated. For in vivo study, peri-implant bone regeneration and the osseointegration at the bone-implant interface in femur were also investigated in a rat model.

2. Experiment

2.1. Material preparation

Mg-3 wt.%Zn powder (99.9%, −180 mesh, Tangshan Weihao,

Peer review under responsibility of KeAi Communications Co., Ltd.
* Corresponding author.
** Corresponding author.
E-mail addresses: ouyangsihui@csu.edu.cn (S. Ouyang), hql1990@163.com (Q. Huang), yonliu@csu.edu.cn (Y. Liu), ouyangzhengxiao@csu.edu.cn (Z. Ouyang), liang_luxin@163.com (L. Liang).

https://doi.org/10.1016/j.bioactmat.2018.12.001
Received 28 October 2018; Received in revised form 4 December 2018; Accepted 4 December 2018
Available online 11 December 2018

China) and Pure Ti powder (99.5%, −325 mesh, Xi'an Sailong, China) were used as raw materials. Mg−3Zn powder was mixed in volume percent of 20% with Ti powder under argon atmosphere for 8 h. The samples were marked as Ti−Mg MMCs. The mixed powder was filled into graphite molds with diameter of 20 mm, and then sintered by using SPS-D 25/3 (FCT Systeme GmbH, Germany) under a vacuum of 10^{-3} Pa. The mixed powders were pre-pressed with a load of 40 MPa and then heated to 650 °C for 5 min. The heating rate was 100 °C/min. The as-sintered Ti−Mg MMCs (diameter: 20 mm, thickness: 10 mm) were machined into disk-shaped and cylindrical samples. The disk samples (diameter: 14.5 mm, thickness: 1 mm) were used for biocompatibility and immersion tests. The cylindrical ones with a diameter of 2 mm and a length of 3 mm were used for compression tests. Other cylindrical samples with a diameter of 2 mm and a length of 5 mm were used for in vivo tests.

2.2. Microstructural characterization and compression tests

Microstructures of Ti−Mg MMCs were observed by Quanta FEG 250 scanning electron microscope (SEM) with an energy dispersive spectroscopy (EDS) attachment. X-ray diffractometer (XRD, Rigaku D/MAX-2250) with a Cu-K_α radiation was used to identify the phase composition. Compression tests were conducted by MTS Alliance RT with the crosshead speed of 0.5 mm/s at room temperature.

2.3. In vitro study

2.3.1. Immersion tests

The samples were soaked in simulated body fluid (SBF) at 37 °C, and the ratio of the samples to solution was 1 cm^2 to 20 ml. The solutions were analyzed by ICP-AES (IRZS Advantage 1000) at different time intervals. After 3 weeks of immersion, the corrosion products on sample surfaces were removed. Thereafter, the samples were cleaned, dried and observed by SEM.

2.3.2. Cell growth evaluation

SaOS-2 cells were cultured in McCoy's 5A medium containing 15% fetal bovine serum (FBS), 100 U ml^{-1} penicillin and 100 μg mL^{-1} streptomycin at 37 °C in a humidified atmosphere of 5% CO_2. Cell cultured was using the 100% extracts of metal plates, prepared with a surface area to extraction medium ratio of 1.25 ml cm^{-2} in a humidified atmosphere, with 5% CO_2 at 37 °C for 24 h. The supernatant fluid was withdrawn, centrifuged and kept at 4 °C prior to use. Cell viability was measured using Counting Kit-8 (CCK-8, Dojindo, Kumamoto, Japan) assay for 1, 2 and 3 days. The spectrophotometrical absorbance of samples was measured at the wavelength of 450 nm with a microplate reader (Model 680; Bio-RAD, USA).

2.3.3. Alkaline phosphatase (ALP) activity

After culturing for 3, 7 days, the cells were washed three times with PBS and then lysed in RIPA cell lysis buffer (Beyotime, China). The ALP activity was measured by ALP testing kit (Jiancheng bio-engineering research institute of Nanjing, China) and then normalized by the total protein content determined with the BCA assay kit (Beyotime, China).

2.4. In vivo study

2.4.1. Surgical procedure

A rat model with femur condyle defect was used to evaluate the in vivo performance of Ti−Mg MMCs and Ti implants (diameter: 2 mm, length: 5 mm). Six adult white rats obtained from the Second Xiangya Hospital were divided into two groups. The rats were anesthetised by injecting 3% Nembutal (30 mg/kg), and then drilled circular holes 2.2 mm in diameter and 5 mm deep by using a surgical electronic drill. Circular holes were thoroughly rinsed with physiological saline to remove shards of bone. The samples and surrounding tissues were analyzed at 3 weeks after surgery. After being fixed in 10% buffered formalin for 24 h, the tissue samples were paraffin-embedded and then stained hematoxylin for 1 min and eosin for 5 min.

2.4.2. Micro computed tomography analysis

Distal femurs with implants were collected under aseptic conditions, fixed in 4% paraformaldehyde for 2 days, and then rinsed with running water for 24 h. For the assessment of the bone architecture around the different implants after 3 months of implantation, femur condyles with implants were examined using a desktop micro X-ray computed tomography (micro-CT; GE Locus SP, American) machine equipped with an 80 kV X-ray source with a camera pixel size of 15 mm. During scanning, the femur condyles were placed in polyethylene tubes filled with 75 vol % alcohol. Micro-CT images along the transection planes in the region around the implant were obtained. The scans resulted in reconstructed data sets with a voxel size of 28.79 mm. To determine the trabecular volume of interest (VOI) in the axial direction, the region of interest was chosen with its closest edge at 4.0 mm distally from the growth plate. The bone volume (BV, mm^3), total volume (TV, mm^3), bone volume fraction (BV/TV, %), bone surface/bone volume (BS/BV, 1/mm) and trabecular thickness (Tb.Th, mm) were calculated as assessment of trabecular bone mass and its distribution to investigate the in vivo performance of implants on bone formation.

2.5. Statistical analysis

All quantitative data were expressed as the mean ± standard deviation. All assays of in vitro study were repeated three times. Statistical differences were determined by an analysis of variance. $P < 0.05$ was considered statistically significant.

3. Results and discussion

3.1. Microstructures and phase composition

The morphology of Ti−Mg MMCs was shown in Fig. 1. It can be observed that Ti−Mg MMCs synthesized by SPS were dense, and the bonding of Ti and Mg−Zn area appeared to be strong. The EDS line scan results showed the interfacial elemental distributions between two different areas (Fig. 1b). The white area was defined as pure Ti. The Ti grains exhibited an average size of 10 μm. The black area was defined as Mg−Zn area, the size of Mg−Zn area was in the range of 30–100 μm. In addition, Mg−Zn areas were homogeneously distributed among Ti matrix.

The phase composition was identified by XRD, the major phase is α-Ti, the characteristic peaks of Mg and a small amount of MgO phase were also noticed (Fig. 2). Combing the results of XRD and EDS analysis, the composites were composed primarily of Ti and Mg. No intermediate phase formed between Ti and Mg−Zn area. In the phase diagram of Ti−Mg, Ti and Mg are immiscible. Furthermore, the melting point of Ti (1678 °C) is much higher than that of Mg (649 °C). Therefore, it is hard to obtain Ti−Mg composites via the traditional casting methods. SPS can consolidate powders with non-equilibrium and immiscible structures, showing unique advantages over other methods for preparing metal-metal composites. In general, Ti−Mg MMCs with dense microstructure were successful synthesized by SPS in this work.

The compressive properties of Ti−Mg MMCs were shown in Table 1. The yield stress and ultimate tensile strength (UTS) of Ti−Mg MMCs were measured to be 634.2 and 1156.8 MPa, respectively. The breaking elongation of Ti−Mg MMCs was around 20%. The results indicate that Ti−Mg MMCs exhibited good mechanical properties.

Fig. 3 showed the morphology of pores generated on the surface of Ti−Mg MMCs after being soaked in SBF for 3 weeks. The shape of the pores was consistent with that of Mg−Zn areas. The Mg−Zn areas were in direct contact with Ti. Thus, the composite structure could suffer from the galvanic corrosion. The electrode potential of Mg−3Zn alloy is

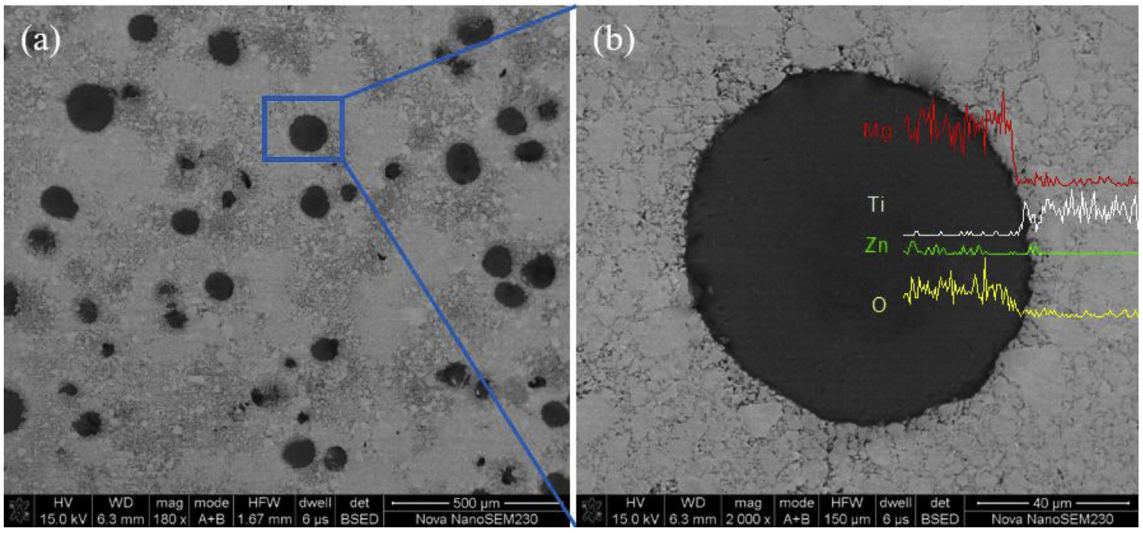

Fig. 1. (a) SEM images and (b) EDS line scan results of Ti—Mg MMCs.

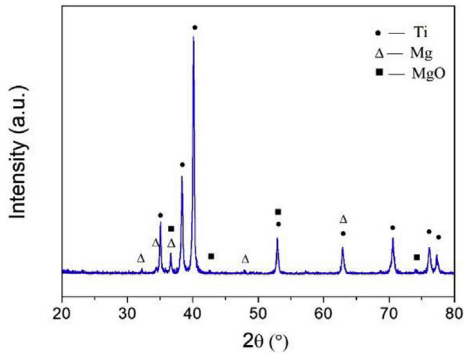

Fig. 2. The XRD pattern of Ti—Mg MMCs.

Table 1
The compressive properties of Ti—Mg MMCs.

Composition	Yield Stress (Mpa)	UTS (Mpa)	Strain at fracture (%)
Ti—Mg MMCs	634.2 ± 23.8	1156.8 ± 186.7	19.7 ± 0.2

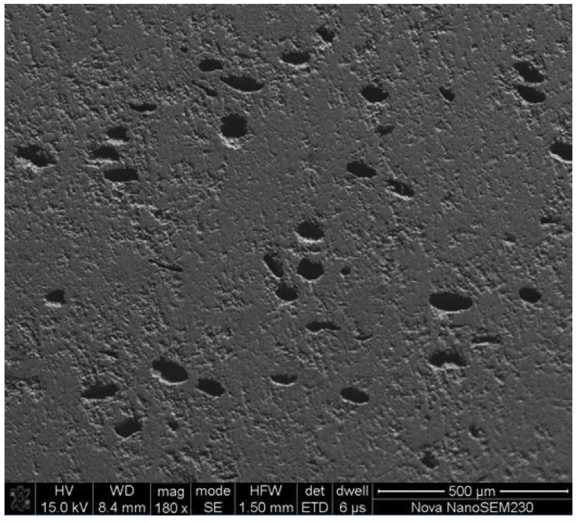

Fig. 3. The morphology of Ti—Mg MMCs after immersion test in SBF.

lower than that of Ti [19,20]. Therefore, the Mg—Zn areas were corroded, and the pores were left within the surface of Ti matrix. The size of pores ranged from 50 to 120 µm, and was a little larger than that of Mg—Zn area. According to some reports, the pore size of 75–100, 140 and 200–300 µm could promote osteoinduction and osteointegration [21,22]. In general, the pore size which range from 100 to 400 µm is proper to allow bone tissue to adhere, proliferate and remodel inside the pores [23].

The released kinetics of Mg^{2+} and Zn^{2+} from Ti—Mg MMCs were shown in Fig. 4. The concentration of Mg^{2+} and Zn^{2+} both increased with prolonged immersion time. During the first 3 days, the release rates of Mg^{2+} and Zn^{2+} were relatively fast. Till 14 days, the concentrations of Mg^{2+} and Zn^{2+} remained almost unchanged for longer durations.

3.2. Cell proliferation and differentiation

SaOS-2 cells were cultured by Ti and Ti—Mg MMCs extraction medium, respectively. The SaOS-2 cell viability was measured by CCK-8 assay at day 1, 2 and 3 (Fig. 5). The viability of SaOS-2 cells grown in Ti—Mg MMCs extraction medium was higher than that of Ti group all the time. Compared to Ti group, Ti—Mg MMCs extraction medium promoted the proliferation of SaOS-2 cells.

The differentiation of SaOS-2 cells was evaluated by ALP activity. The ALP activity can imply the differentiation of osteoblasts at early stage. It is commonly defined as the amount of phenol catalyzed by 1 milligram of proteins per minute at 37 °C (U/mg protein). As shown in Fig. 6, the ALP activity of SaOS-2 cells cultured by Ti—Mg MMCs extraction medium was higher than that of Ti group. In our previous work, when Ti—Mg composites were soaked in SBF, Mg^{2+} released from the composites into the solution, and the concentration of Mg^{2+} increased with prolonged soaking duration [16]. Huang et al. [24] investigated the proliferation and differentiation of SaOS-2 cells in response to exogenous Mg^{2+}. The results showed that Mg^{2+} at an appropriate concentration range exhibited stimulatory effect on SaOS-2 cell response. Therefore, when SaOS-2 cells were cultured on Ti—Mg MMCs, Mg^{2+} released from Ti—Mg MMCs is considered as an important factor in promoting the proliferation and differentiation of SaOS-2 cells. In addition, Zn is also known to promote osteogenesis. Therefore, the release of Zn from Mg—Zn area may also contribute to the enhanced proliferation and ALP activity.

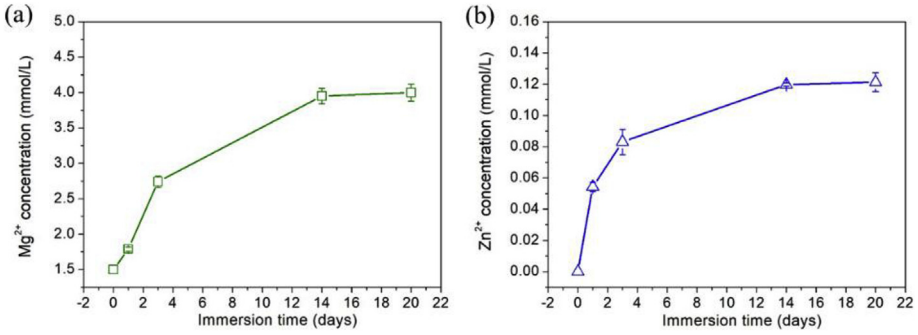

Fig. 4. Ion concentrations of Ti—Mg MMCs immersed in SBF for various durations: (a) Mg^{2+}; (b) Zn^{2+}.

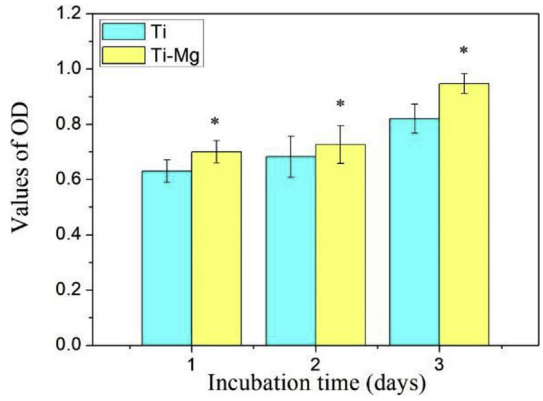

Fig. 5. The CCK-8 assay of SaOS-2 cells cultured by Ti and Ti—Mg MMCs extraction medium for 1, 2 and 3 days (*P < 0.05, compared with Ti).

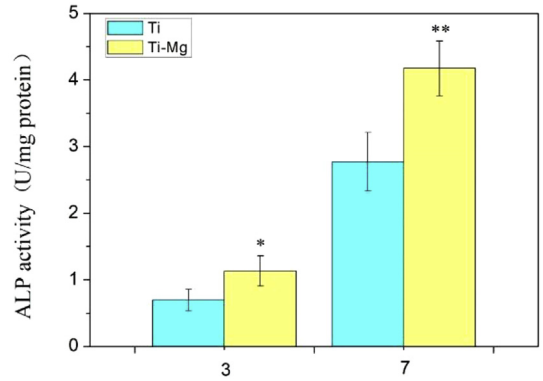

Fig. 6. The ALP activity of SaOS-2 cells cultured by Ti and Ti—Mg MMCs extraction media for 3 and 7 days (*P < 0.05, * *P < 0.01, compared with Ti).

3.3. Micro-CT image analysis

Fig. 7 showed the micro-CT images of cross section and longitudinal section in the region around the implants after 3 weeks of implantation. Micro-CT imaging can provide valuable information on the integrity of the entire implant. It can be observed that Ti and Ti—Mg implants could maintain the mechanical integrity, and Ti—Mg implant had rougher surface than Ti implants, after 3 weeks of implantation. The average thickness value of the Ti—Mg MMCs-bone interface was 0.12 mm higher than that of the Ti-bone interface (Fig. 7b).

The parameters of trabecular in the axial direction were shown in Fig. 8. The BV, BV/TV, Tb.Th values of Ti—Mg MMCs were increased by 19.6, 13.5 and 17.9% compared to those of Ti, respectively. It indicates that the bone formation around Ti—Mg implant was promoted than that around Ti implant. In addition, Ti—Mg group had higher level of Tb.Th than Ti group, suggesting that the structure of bone trabecula around

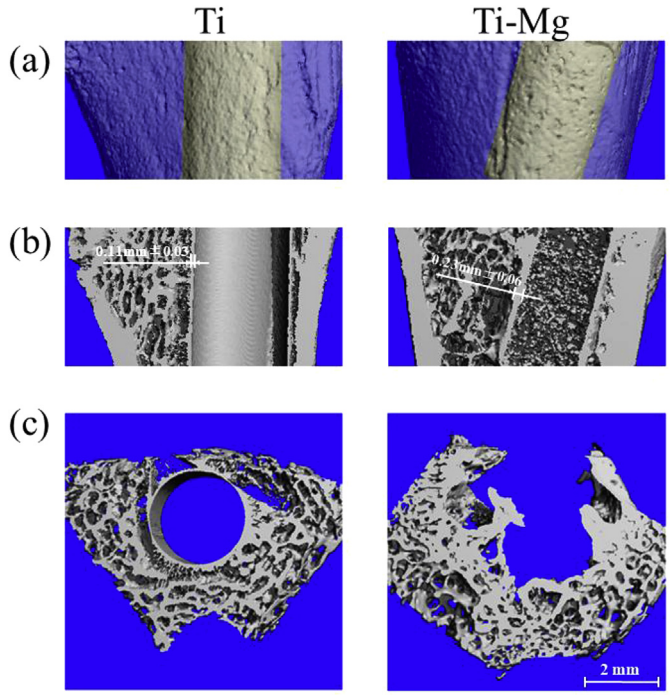

Fig. 7. Micro-CT analysis of femoral condyle containing pure Ti and Ti—Mg MMCs implants at 3 week: (a) micro-CT reconstruction images of femoral condyle with implants (b) without implants and (c) cross section of femoral condyle.

implanted Ti—Mg was more mature than that around implanted Ti. The BS/BV of Ti—Mg group was decreased by 16.7% compared to that of Ti group, also indicating that volume of bone around Ti—Mg implant increased more than that around Ti implant.

3.4. Hematoxylin-eosin (H&E) staining analysis

Fig. 9 further showed the staining of interface between implants and bone tissue. The Ti group, as permanent implant material, can maintain its original shape, after being implanted in rats. The results indicated that the implanted Ti—Mg significantly increased the number of trabecula attached to the surfaces than control. In addition, new bone can be found on the surface of implanted Ti—Mg and had much closer contact with implanted Ti—Mg. Therefore, the interaction between implanted Ti and surrounding bone tissue is considered to be weaker than that of the Ti—Mg MMCs group. In general, the osseointegration around Ti—Mg MMCs was found to be stronger than that around Ti.

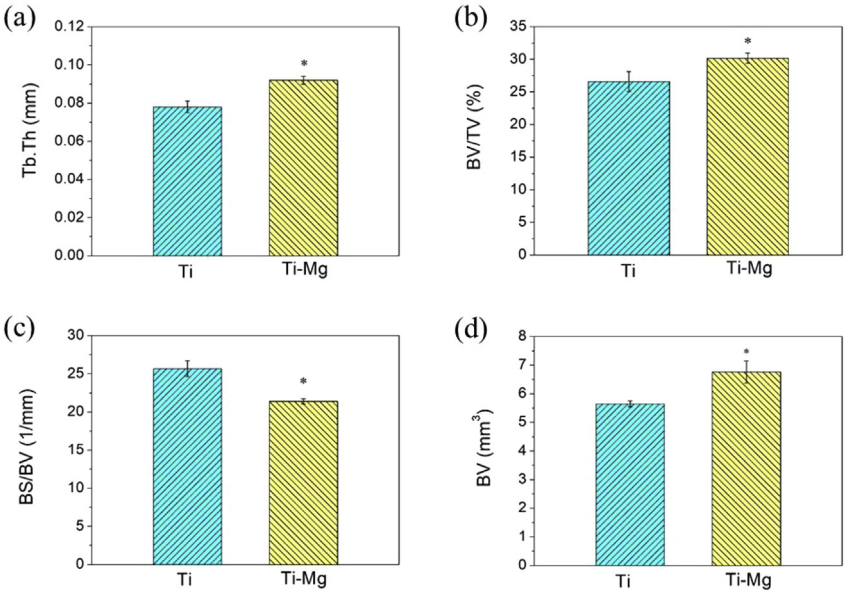

Fig. 8. Quantitative analyses of trabecular volume of Ti and Ti−Mg in axial direction revealing bone parameters: (a) Tb.Th; (b) BV/TV; (c) BS/BV; (d) BV(*P < 0.05, compared with Ti).

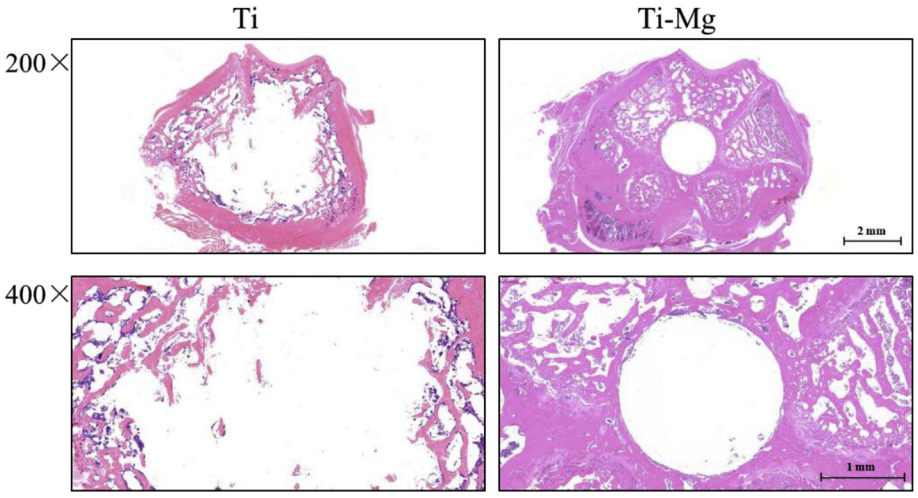

Fig. 9. H&E staining of interface between implants and bone tissue (magnification: 200/400).

4. Conclusions

In the current work, Ti−Mg MMCs were fabricated by SPS. The in vitro and in vivo biological performances of Ti−Mg MMCs were investigated by taking pure Ti as the control group. Two main findings were listed as below:

(1) In vitro assay showed that Ti−Mg MMCs exhibited excellent cytocompatibility, evidenced by the promoted proliferation and ALP activity of SaOS-2 cells.
(2) In vivo study showed that Ti−Mg MMCs enhanced in vivo osseointegration compared to Ti, evidenced by the promoted periimplant bone regeneration and interfacial reactions.

Conflict of interest

All authors have reviewed the final version of the manuscript and approve it for publication, and there is on conflict of interest in this work.

Acknowledgments

The authors gratefully acknowledge the support from the National Natural Science Funds for Distinguished Young Scholar of China (51625404) and China Postdoctoral Science Foundation (2018M630909).

References

[1] M. Geetha, A.K. Singh, R. Asokamani, A.K. Gogia, Ti based biomaterials, the ultimate choice for orthopaedic implants – a review, Prog. Mater. Sci. 54 (2009) 397–425.
[2] L. Kunčická, R. Kocich, T.C. Lowe, Advances in metals and alloys for joint replacement, Prog. Mater. Sci. 88 (2017) 232–280.
[3] M. Niinomi, Titanium alloys, in: R. Narayan (Ed.), Encyclopedia of Biomedical Engineering, Elsevier, Oxford, 2019, pp. 213–224.
[4] L. Lin, H. Wang, M. Ni, Y. Rui, T. Cheng, C. Cheng, X. Pan, G. Li, C. Lin, Enhanced osteointegration of medical titanium implant with surface modifications in micro/nanoscale structures, J. Orthopaed. Transl. 2 (2014) 35–42.
[5] C. Treves, M. Martinesi, M. Stio, A. Gutiérrez, J.A. Jiménez, M.F. López, In vitro biocompatibility evaluation of surface-modified titanium alloys, J. Biomed. Mater. Res. 92 (2010) 1623.
[6] H. Ao, Y. Xie, S. Yang, X. Wu, K. Li, X. Zheng, T. Tang, Covalently immobilised type I collagen facilitates osteoconduction and osseointegration of titanium coated

implants, J. Orthopaed. Transl. 5 (2016) 16–25.
[7] Y.F. Zheng, X.N. Gu, F. Witte, Biodegradable metals, Mater. Sci. Eng. R Rep. 77 (2014) 1–34.
[8] X. Li, X. Liu, S. Wu, K.W.K. Yeung, Y. Zheng, P.K. Chu, Design of magnesium alloys with controllable degradation for biomedical implants: from bulk to surface, Acta Biomater. 45 (2016) 2–30.
[9] T. Kraus, S.F. Fischerauer, A.C. Hänzi, P.J. Uggowitzer, J.F. Löffler, A.M. Weinberg, Magnesium alloys for temporary implants in osteosynthesis: in vivo studies of their degradation and interaction with bone, Acta Biomater. 8 (2012) 1230–1238.
[10] S. Zhang, Y. Bi, J. Li, Z. Wang, J. Yan, J. Song, H. Sheng, H. Guo, Y. Li, Biodegradation behavior of magnesium and ZK60 alloy in artificial urine and rat models, Bioact. Mater. 2 (2017) 53–62.
[11] S. Zhang, Y. Zheng, L. Zhang, Y. Bi, J. Li, J. Liu, Y. Yu, H. Guo, Y. Li, In vitro and in vivo corrosion and histocompatibility of pure Mg and a Mg-6Zn alloy as urinary implants in rat model, Mater. Sci. Eng. C 68 (2016) 414–422.
[12] N. Li, Y. Zheng, Novel magnesium alloys developed for biomedical application_ a review, J. Mater. Sci. Technol. 29 (6) (2013) 489–502.
[13] H. Chouirfa, H. Bouloussa, V. Migonney, C. Falentin-Daudré, Review of titanium surface modification techniques and coatings for antibacterial applications, Acta Biomater. (2018), https://doi.org/10.1016/j.actbio.2018.10.036 PII: S1742-7061(18)30635-4.
[14] Z. Esen, B. Dikici, O. Duygulu, A.F. Dericioglu, Titanium–magnesium based composites: mechanical properties and in-vitro corrosion response in Ringer's solution, Mater. Sci. Eng., A 573 (2013) 119–126.
[15] S. Jiang, L.J. Huang, Q. An, L. Geng, X.J. Wang, S. Wang, Study on titanium-magnesium composites with bicontinuous structure fabricated by powder metallurgy and ultrasonic infiltration, J. Mech. Behav. Biomed. 81 (2018) 10–15.
[16] Y. Liu, K. Li, T. Luo, M. Song, H. Wu, J. Xiao, Y. Tan, M. Cheng, B. Chen, X. Niu, R. Hu, X. Li, H. Tang, Powder metallurgical low-modulus Ti–Mg alloys for biomedical applications, Mater. Sci. Eng. C 56 (2015) 241–250.
[17] L. Jia, S. Li, H. Imai, B. Chen, K. Kondoh, Size effect of B4C powders on metallurgical reaction and resulting tensile properties of Ti matrix composites by in-situ reaction from Ti–B4C system under a relatively low temperature, Mater. Sci. Eng., A 614 (2014) 129–135.
[18] S. Tkachenko, J. Cizek, R. Mušálek, K. Dvořák, Z. Spotz, E.B. Montufar, T. Chráska, I. Křupka, L. Čelko, Metal matrix to ceramic matrix transition via feedstock processing of SPS titanium composites alloyed with high silicone content, J. Alloy Compd. 764 (2018) 776–788.
[19] X. Li, X. Liu, S. Wu, K.W.K. Yeung, Y. Zheng, P.K. Chu, Design of magnesium alloys with controllable degradation for biomedical implants: from bulk to surface, Acta Biomater. 45 (2016) 2–30.
[20] S. Jiang, L.J. Huang, Q. An, L. Geng, X.J. Wang, S. Wang, Study on titanium-magnesium composites with bicontinuous structure fabricated by powder metallurgy and ultrasonic infiltration, J. Mech. Behav. Biomed. 81 (2018) 10–15.
[21] J. Li, H. Liao, B. Fartash, L. Hermansson, T. Johnsson, Surface-dimpled commercially pure titanium implant and bone ingrowth, Biomaterials 18 (1997) 691–696.
[22] H.E. Götz, M. Müller, A. Emmel, U. Holzwarth, R.G. Erben, R. Stangl, Effect of surface finish on the osseointegration of laser-treated titanium alloy implants, Biomaterials 25 (2004) 4057–4064.
[23] Y. Li, N. Chen, H. Cui, F. Wang, Fabrication and characterization of porous Ti–10Cu alloy for biomedical application, J. Alloy Compd. 723 (2017) 967–973.
[24] Q. Huang, X. Li, T. Liu, H. Wu, X. Liu, Q. Feng, Y. Liu, Enhanced SaOS-2 cell adhesion, proliferation and differentiation on Mg-incorporated micro/nano-topographical TiO 2 coatings, Appl. Surf. Sci. 447 (2018) 767–776.